Numerical and experimental study of the dynamic behaviour of Cork

Celina Pires Gameiro, José Cirne, Gérard Gary, Victor Miranda, Joaquim Pinho-Da-Cruz, Filipe Teixeira-Dias

Numerical and Experimental Study of the Dynamic Behaviour of Cork

C.P. Gameiro[a,†], J. Cirne[a], G. Gary[b], V. Miranda[c], J. Pinho-da-Cruz[c] and F. Teixeira-Dias[c]

[a] *CEMUC – Departamento de Engenharia Mecânica*
Faculdade de Ciências e Tecnologia da Universidade de Coimbra
3030-201 Coimbra
Portugal

[b] *Laboratoire de Mécanique des Solides*
Ecole Polytechnique
91128 Palaiseau
France

[c] *Departamento de Engenharia Mecânica, Universidade de Aveiro*
Campus Universitário de Santiago
3810-193 Aveiro
Portugal

[†]Corresponding author: celina.gameiro@dem.uc.pt

Abstract. *Cork is a natural cellular material with increasing industry applications due to its remarkable combination of properties. Its mechanical behaviour explains why it is often used for applications like sealing, packaging, insulation, vibration control, weight reduction, flotation, sound dampening and many others. However, the mechanical behaviour of cork when subjected to impact has not been well investigated yet. In the present work, the authors compare the quasi-static and dynamic response of four types of cork when compressed axially at strain rates from 10^{-3} s^{-1} to 600 s^{-1}. Furthermore, in order to analyse the possible benefits to use the different types of cork in lightweight absorbing-energy structures, aluminium cork-filled tubes and their empty counterparts are tested experimentally and numerically at some quasi-static and dynamic strain rates under axial compressive loading. Data from the Split-Hopkinson Pressure Bar are used to generate stress-strain curves for natural and agglomerate cork samples. The numerical simulations of the dynamic compression of the specimens are performed using the finite element method software LS-DYNA^{TM} and show quite good agreement with the experimental results. In order to investigate the possible advantages of cork-filling in longer tubes with a different section, the authors also simulate the influence of the introduction of agglomerate cork in square aluminium tubes. For the cork-filled structures, when compared with the empty aluminium tubes, greater crushing forces and energy absorption capacities are observed (experimentally and numerically) for high values of the strain. The square structures analysed numerically, when filled with cork, show greater values of energy absorption since the beginning of the deformation process.*

Keywords: Cork; impact; mechanical behaviour; experimental testing; numerical simulation.

1 INTRODUCTION

In the last few years, cellular materials have been playing a very important role in industrial applications because they may have good energy absorption capabilities, as well as important advantages such as damping, insulation, specific stiffness and fire retar

dant properties. Actually, under compressive loading, cellular material can undergo large strain deformation while maintaining its low stress level before the densification, which allows them to absorb large amounts of energy. Nevertheless, the properties of foams can vary significantly by the choice of the cell wall material, the volume fraction of the solid, the geometry and the strain rate of the loading. Hence, many authors have been trying to characterize those materials under quasi-static and dynamic loading [1, 2, 3]. The filling of tubular structures with lightweight metallic foams in order to improve their energy absorption has also taken considerable interest. Santosa *et al.* [4] found that the increase of the mean crushing force of a filled column has a linear dependence with the foam compressive resistance and cross-sectional area of the column. The mechanical behaviour of different types of foams used as filler in aluminium tubular structures, under static and dynamic loading, has been studied extensively in the last few years [5, 6]. Generally, there is a significant increase of the average crushing force and, in some cases, a change of the deformation behaviour is observed because of the interaction effect between the tube and the foam [7, 8]. Aktay *et al.* [9], among others, also developed a numerical study of the crushing of thin-walled aluminium tubes with foam used as filler, and validated adequate models for filled structures.

Cork is a quite complex natural cellular material, with quite unknown or not well understood properties. The fundamental aspects of the mechanical behaviour of cork under axial compressive loading have already been studied by several authors [10-13]. However, the mechanical behaviour of cork when subjected to impact has not been well investigated yet since the studies described in the literature generally focus strain rates inferior to 10^{-1} s^{-1}.

Hence, this work pretends to be a start for the study of the mechanical behaviour of cork under impact loading. The quasi-static (at 10^{-3} s^{-1}) and the dynamic behaviour of cork (strain rates from 200 to 600 s^{-1}) were compared and the possible influence of the cork type, the density, the humidity, the cellular structure and the strain rate was examined. In order to analyse the cork energy-absorption capabilities, circular cork-filled aluminium tubes of different lengths were compressed at different static and dynamic strain rates. Finally, numerical simulations of the dynamic compressive tests realized experimentally were performed and the behaviour of square aluminium tubes with and without a cork-filler was also predicted. The numerical simulations were carried out using the finite element code LS-DYNA™, and globally showed good agreement with the experimental results.

2 EXPERIMENTAL TESTS

2.1 The Cork Structure

In order to characterize the cork structure, the authors usually refer to three principal directions which define the orientation of the material in the oak: directions along the radius and the axis of the trunk, respectively designated by radial and axial, and the tangential direction to the circumference.
As other cellular materials, cork is composed of closed cells, which represent approximately 15% of the total volume of the material and form a three-dimensional structure in space [10]. The cells aspect was observed in three directions, respectively perpendicular to the three principal directions already defined, with electronic scanning devices. The cork cells can be defined as prisms, globally hexagonal, which form columns in the radial direction. The cell walls in this direction present significant corrugations, so that the cells are shaped like a concertina (Figure 1).

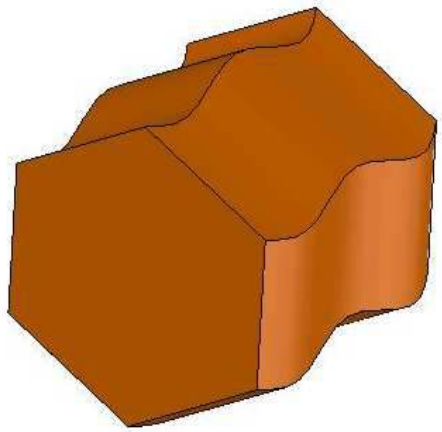

Figure 1: Cork cell.

2.2 Materials

The particular structure of the cork, as a consequence of the cork cells shape, explains the choice of the samples used for the static and dynamic uniaxial compressive tests. Hence, the specimens used were removed from the oak in the radial direction and in another of the two non-radial directions because a similar compressive behaviour may be expected in the axial and tangential directions. For the static and dynamic tests, natural radial (R) and non-radial (NR) cork cylinders, as well as agglomerate (A) and micro-agglomerate (MA) cylindrical cork samples were used. The objective of this choice was to compare the performance of agglomerate material, produced industrially and available in many shapes and sizes, with the behaviour of a natural material characterized by much more variable properties and which is more difficult to use in industrial applications because of its shorter size. The agglomerate cork tested is called "composed agglomerate" and is made of 3 to 6 mm

cork particles joined with an adhesive. The micro-agglomerate cork contains smaller 0.5 to 2 mm cork particles.
The cork samples produced by ROCAP were cylinders with an average diameter of 22.8 mm and an average length of 51.0 mm, except the radial cork cylinders which could not have a length higher than 26.2 mm because of the fact they were removed from the interior to the exterior of the bark (Figure 2). Moreover, all the specimens were extracted from the same cork-oak, or from neighbour cork-oaks, in order to limit as much as possible the variations of the structure and of the quality of the cork.

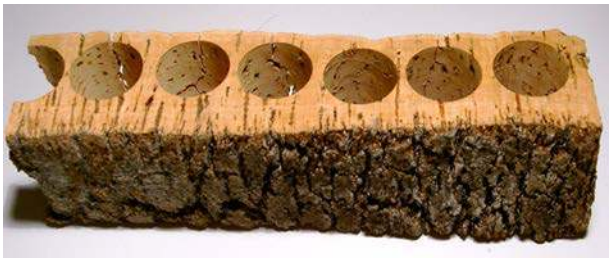

Figure 2: Corktree bark.

An automatic system from EGITRON, called "Medcork", used for the measurement of cork stoppers, allowed to display the length, the average diameter, the ovality, the density and the humidity of each sample. Some discs of radial cork were also provided: some had an approximate diameter of 35 mm and a thickness of 7 mm, whereas others had an approximate diameter of 27 mm and a thickness of 6 mm. For technical reasons, inherent to the fact that the Medcork is not prepared for short cylinders, the values of humidity and ovality for the discs were not displayed. After the measurements, some of the specimens were cut off from the cylinders, according to the needs of the tests performed, and weighed again.
The circular tubes used to fill the four types of cork had an outer diameter of 25 mm, a thickness of 1.5 mm and were cut for lengths of 25 and 50 mm. The aluminium alloy (more than 99% Al) was in accordance with the standard AW 6060/6063 and was submitted to a T5 heat treatment. A tensile test performed in a hydraulic testing machine INSTRON 4204 gave the quasi-static stress-strain curve displayed in Figure 3. The alloy tested presented a yield stress of 160 MPa approximately.
The tubes, with and without cork filler, were weighed with a 0.01 g precision in an electronic balance FX-3000 from AND. The cork was introduced inside the tubes with a slight compression (approximately 0.5 mm) which did not damage the cork cells.

2.3 Static Tests

The quasi-static uniaxial compressive tests on cork and on the tubular aluminium structures, with and without cork filler, were realized in a hydraulic testing machine INSTRON 4206, with a load cell capacity of 100 kN. The load speed was fixed at 1.5 mm/min. Hence, 15 mm and 20 mm length cylinders of radial, non-radial, agglomerate and micro-agglomerate cork were tested at strain rates of 1.6×10^{-3} s^{-1} and 1.25×10^{-3} s^{-1}. The tubular structures with 25 mm and 50 mm were respectively tested at 10^{-3} s^{-1} and 5×10^{-4} s^{-1}. The geometry of the samples tested are presented in Figure 4.

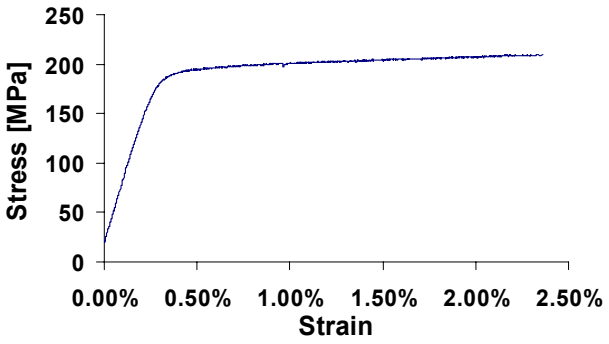

Figure 3: Aluminium stress-strain curve.

Figure 4: Geometry of the tested samples.

The list of the specimens tested with the hydraulic testing machine is shown in Tables 1 to 3. For all the specimen tested, "T" refers to tube, "V" refers to empty tubes, "A" to agglomerate, "MA" to micro-agglomerate, "NR" to non-radial, "R" to radial, "D" to dynamic and "E" to static. The last number always corresponds to the position of the sample in a same series. Hence, the sample T50MAE1 is the first 50 mm tube tested statically with micro-agglomerate cork used as filler.

2.4 Dynamic Tests

2.4.1 Brief introduction to the Split Hopkinson Pressure Bar (SHPB)

The cork and the tubular structures were dynamically tested on Split Hopkinson Pressure bars. In order to make a dynamic compression test with a SHPB, a short specimen is inserted between two identical bars with a higher yield stress than the tested material. Strain gages are cemented to the bars. With the impact of a striker, a longitudinal compressive elastic wave is induced in the incident bar. A part of this wave is reflected at the interface bar/sample while the other part is transmitted through the specimen and induces an elastic wave in the output

Table 1: Static cork samples.

Sample	Length [mm]	Weight [g]	Medcork Reference
15AE1	15.40	1.86	B17
15AE2	15.00	1.80	B17
15AE3	15.20	1.78	B17
15MAE1	15.20	1.80	A17
15MAE2	15.30	1.82	A17
15MAE3	15.10	1.82	A17
15NRE1	14.80	0.98	E14
15NRE2	15.40	1.05	E13
15NRE3	15.00	1.02	E13
15RE1	15.00	0.90	H3
15RE2	15.60	0.93	H5
15RE3	15.30	0.98	H6
20AE1	20.50	1.27	B18
20AE2	19.80	1.24	B18
20AE3	20.00	1.23	D2
20MAE1	20.00	2.40	I2
20MAE2	20.10	2.45	A18
20MAE3	20.00	2.45	A18
20NRE1	20.20	1.37	E16
20NRE2	20.30	1.43	E16
20NRE3	20.20	1.30	E17
20RE1	20.20	1.27	H4
20RE2	20.60	1.24	H2
20RE3	20.60	1.23	H1

bar, as shown in Figure 5 [14].

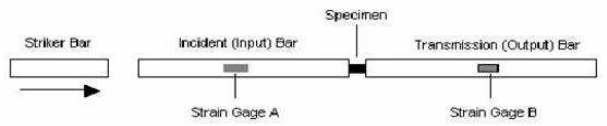

Figure 5: Split Hopkinson Pressure Bar.

The elementary analysis of the waves is based on two simplifying hypothesis: the one dimensionality of the waves in bars and the homogeneity of the forces and strains in the specimen. The hypothesis of one-dimensional wave propagation induces the direct relation between the strains measured by strain gages, and the stresses in the specimen, and also the strain rate associated to the movement of the sample faces. If one assumes that elastic waves propagate without dispersion, the forces and the displacements at the bar/specimen interfaces can easily be calculated. Assuming then that the stresses and the strains are homogeneous in the specimen, the average behaviour of the material tested can be found.
Let ε_i and ε_r be elastic strains developed by the incident and reflected waves and measured by the strain gage A, and ε_t the strain developed by the transmitted wave, measured by the strain gage B. Assuming that the strain at the interfaces can be found by a simple time shift, and that all the hypothesis described before are verified, one can obtain the following expressions (1).

Table 2: Static tubes samples.

Tube	Length [mm]	Weight [g]	Medcork Reference
T25VE1	25.00	7.74	-
T25VE2	25.00	7.70	-
T25VE3	25.00	7.74	-
T25AE1	25.00	10.66	B1
T25AE2	25.00	10.81	B2
T25AE3	25.00	10.68	B2
T25MAE1	25.00	10.89	A1
T25MAE2	25.00	10.81	A2
T25MAE3	25.00	10.76	A1
T25NRE1	25.00	9.43	E2
T25NRE2	25.00	9.61	E2
T25NRE3	25.00	9.42	E1
T25RE1	25.00	9.54	H13
T25RE2	25.00	9.38	H14
T25RE3	25.00	9.53	H15
T50VE1	50.00	15.58	-
T50VE2	50.00	15.57	-
T50VE3	50.00	15.54	-
T50AE1	50.00	21.46	B19
T50AE2	50.00	21.49	B11
T50AE3	50.00	21.68	B15
T50MAE1	50.00	21.73	A10
T50MAE2	50.00	21.71	A14
T50MAE3	50.00	21.75	A12
T50NRE1	50.00	18.89	C20
T50NRE2	50.00	18.92	C16
T50NRE3	50.00	18.93	C9
T50RE1	50.00	18.91	H29+H30
T50RE2	50.00	19.04	H33+H34
T50RE3	50.00	18.96	H31+H32

$$\sigma = E\varepsilon \quad \text{and} \quad v = -C_0\varepsilon \tag{1}$$

where σ is the stress, E is the Young modulus of the bars, C_0 is the speed of the elastic waves in the bars and v is the mass velocity.
Let U_A and U_B respectively be the displacements of the input and output interfaces, and F_A, F_B, V_A e V_B the corresponding forces and velocities.
The velocities of the faces A and B are given by expressions (2).

$$\begin{aligned} V_A(t) &= C_0[\varepsilon_i(t) - \varepsilon_r(t)] \\ V_B(t) &= C_0\varepsilon_t(t) \end{aligned} \tag{2}$$

The forces at the interfaces of the specimen can also be calculated (expressions (3)).

$$\begin{aligned} F_A(t) &= S_E E[\varepsilon_i(t) + \varepsilon_r(t)] \\ F_B(t) &= S_E E\varepsilon_t(t) \end{aligned} \tag{3}$$

where S_E is the cross section of the bars.
Admitting that the stresses and the strains are homogeneous in the specimen, the average strain, the

Table 3: Properties of the tested cork, for each Medcork reference.

Reference	Type of cork	Average diameter [mm]	Ovality [mm]	Density [kg/m^3]	Humidity [% HR]
A1	MA	22.87	0.03	297	5.4
A2	MA	22.85	0	295	6
A10	MA	22.85	0.01	293	6
A12	MA	22.85	0.03	295	6.1
A14	MA	22.83	0.01	299	6
A17	MA	22.87	0.01	292	6
A18	MA	22.89	0.01	291	6
B1	A	22.82	0.02	288	6.5
B2	A	22.84	0.03	291	6.3
B11	A	22.82	0.03	283	6.2
B15	A	22.84	0.01	291	6.2
B17	A	22.81	0	293	6.3
B18	A	22.82	0.04	294	6.4
B19	A	22.84	0.01	281	6.5
C9	NR	22.81	0.03	163	6.9
C16	NR	22.78	0	164	10.2
C20	NR	22.75	0.03	162	9.8
D2	A	22.85	0.01	299	6.3
E1	NR	22.84	0.07	163	9.7
E2	NR	22.81	0.03	174	6.5
E13	NR	22.77	0.04	149	9.7
E14	NR	22.75	0.08	166	6.5
E16	NR	22.79	0.07	172	6.7
E17	NR	22.78	0.06	161	6.9
H1	R	22.77	0.03	154	9.7
H2	R	22.81	0.09	152	9.7
H3	R	22.81	0.01	149	9.7
H4	R	22.79	0.04	157	9.7
H5	R	22.81	0.06	149	9.7
H6	R	22.73	0.03	160	10.2
H13	R	22.8	0.04	175	10.2
H14	R	22.78	0.06	151	9.7
H15	R	22.69	0.06	176	9.6
H29	R	22.76	0	153	7
H30	R	22.72	0.02	168	9.7
H31	R	22.82	0.07	153	7
H32	R	22.75	0.07	174	10.2
H33	R	22.79	0.01	171	6.9
H34	R	22.71	0.03	167	9.8
I2	MA	22.86	0.02	292	6

average strain rate and the average stress in the specimen, as a function of time, are given by the expressions (4), where l_S stands for the specimen length.

$$\begin{aligned} \overline{\varepsilon}(t) &= \frac{U_A(t) - U_B(t)}{l_S} \\ \overline{\dot{\varepsilon}}(t) &= \frac{V_A(t) - V_B(t)}{l_S} \\ \overline{\sigma}(t) &= \frac{F_A(t) + F_B(t)}{2S_E} \end{aligned} \tag{4}$$

These equations correspond to the standard analysis of the test. It appears that the equilibrium of forces can be verified for each test, using expressions (2), and one can assume the hypothesis of homogeneity of stresses and strains in the specimen only when the forces at the sample interface are equal.
However, there are a few limitations and difficulties associated to the SHPB. A main difficulty is the waves dispersion, which means that the speed of the waves depends slightly on their frequency. The model that takes this correction into account was introduced by Pochhammer and Chree and applied by Davies, and completed for viscoelastic bars by Zhao and Gary [15].
Moreover, to avoid the superposition of the waves which suffer several reflections in the bars (there is only one measurement point in each bar), the maximum length of the striker is generally inferior to half the input bar length. Thus, the time of loading τ applied to the specimen is related to the striker length l_{striker} and determines the maximum strain $\varepsilon_{\max}$ considered in the sample for a given strain rate (expressions (5) and (6)).

$$\tau = \frac{2l_{\text{striker}}}{C_0} \tag{5}$$

$$\varepsilon_{\max} = \dot{\varepsilon}\tau \tag{6}$$

Furthermore, another important point is to verify the adequate adaptation of the impedance of the bars and the sample, so that the waves amplitudes in the input and output bars can be great enough to calculate the forces and the velocities with accuracy. Hence, and particularly for the dynamic study of cellular materials with Hopkinson Bars, using viscoelastic bars (nylon for example) with an adequate correction of the dispersion, is a way to prevent a low transmitted signal comparatively with noise. One must also verify the hypothesis of equilibrium of the forces in the interfaces of the sample.
For all the samples tested dynamically in SHPB, the authors used the software DAVID™, created in the LMS, *Laboratoire de Mécanique des Solides (Ecole Polytechnique, France)* by G. Gary and V. De Greef, to treat the results and obtain the stress-strain curves.
For the cork (Figure 6) and tubular samples tested with SHPB, a good equilibrium was observed in the interfaces of the specimens.

2.4.2 Description of the Tests

The four types of cork samples were tested with nylon SHPB (Figure 7), whose characteristics are shown in Table 4.

Figure 6: Cork samples tested with SHPB.

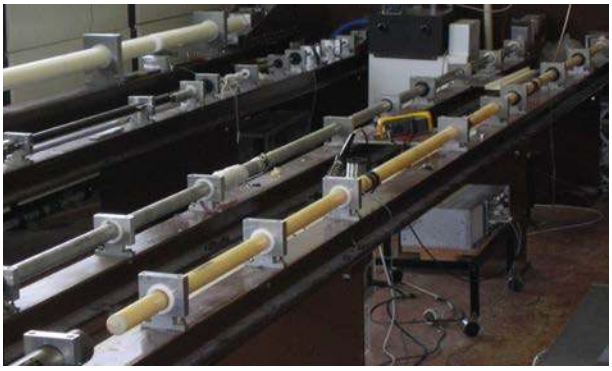

Figure 7: Hopkinson bars of the LMS.

The striker was expelled at 3 and 6 m/s approximately, and originated several strain rates in the samples, from 200 to 600 s^{-1}.
The Table 5 shows the list of the cork samples tested with nylon SHPB, as well as the average strain rate originated in each one of them.
Some of the samples were impacted twice to analyse the effect of a second shock wave on the stress-strain curves obtained. Some of the 25 mm tubes, empty or filled with cork, were tested at impact velocities of 11 and 15 m/s with aluminium SHPB. The characteristics of the bars and the samples are shown in Tables 6 and 7.
As referred above, one of the limitations, inherent to the use of the classic SHPB, is that the strain for which one can obtain values for the stress in the tubes is limited. Hence, the maximum strain is 24% for the 15 m/s impact, and 17% for the 11 m/s impact.
That is the reason why the authors also tested 50 mm aluminium tubes, empty and with cork-fillers, in an equipment device, called "blockbar" which is being developed in the *Laboratoire de Mécanique des Solides (LMS)*. This equipment allows carrying out force-displacement curves for higher strains. Basically, it consists of a nylon bar, equipped with three strain gages and two zimmers. A steel striker impacts directly the sample which is placed strictly before the nylon bar. The analysis of the incident and reflected waves by deconvolution methods [14], associated to the equilibrium hypothesis of the sample, gives the

Table 4: Characteristics of the nylon SHPB.

	Material	Density [kg/m^3]	Diameter [mm]	Length [m]	Distance strain gage/sample [m]
Striker	Nylon	1164.94	40	1.004	
Input bar	Nylon	1145	41.3	3.064	1.55
Output Bar	Nylon	1145	40	1.919	0.394

Table 5: Properties of the dynamic cork samples.

Sample	Length [mm]	Diameter [mm]	Weight [g]	Medcork or density [kg/m^3]	Average strain rate [s^{-1}]
AD11	10.04	22.73	1.21	I3	210
AD12	10.91	22.71	1.32	A18	250
AD21	10.29	22.76	1.22	I2	500
AD22	10.04	22.73	1.22	I3	500
MAD11	10.16	22.71	1.18	D3	250
MAD12	9.75	22.79	1.15	D2	300
MAD21	10.80	22.67	1.27	B18	500
MAD22	9.98	22.73	1.18	D2	500
NRD12	10.04	22.67	0.75	E11	290
NRD13	10.28	22.34	0.61	E12	300
NRD21	10.22	22.47	0.73	E9	550
NRD22	9.71	22.38	0.59	E12	550
NRD14	10.01	22.53	0.66	E11	200
NRD23	10.72	22.32	0.61	E12	500
RD11	6.80	35.13	1.28	194	200
RD12	6.95	35.68	1.46	162	300
RD22	7.08	35.80	1.32	185	580
RD23	6.95	35.48	1.34	195	580
RD24	6.82	34.94	1.13	173	600
RD15	7.08	35.57	1.36	193	250
RD16	7.01	35.49	1.42	204	300

Table 6: Characteristics of the aluminium SHPB.

	Material	Density [kg/m^3]	Diameter [mm]	Length [m]	Distance strain gage/specimen [m]
Striker	Aluminium	2820	40	1.203	
Input bar	Aluminium	2820	40	2.991	1.493
Output Bar	Aluminium	2820	40	1.850	0.335

Table 7: Properties of the tubes tested with aluminium SHPB

Tube	Length [mm]	Diameter or section area	Weight [g]	Medcork reference	Average strain rate [s^{-1}]
T25VTEST	25.00	110.74 mm^2	7.73	–	500
T25AD11	25.00	25 mm	10.82	B3	500
T25MAD12	25.00	25 mm	10.85	A3	500
T25NRD11	25.00	25 mm	9.39	E3	500
T25RD12	25.00	25 mm	9.38	H19	500
T25VD13	25.00	110.74 mm^2	7.73	–	350
T25MAD13	25.00	25 mm	10.76	A5	350
T25NRD12	25.00	25 mm	9.36	E4	350
T25RD13	25.00	25 mm	9.43	H23	350
T25AD12	25.00	25 mm	10.86	B3	350

Table 8: Blockbar characteristics.

	Material	Density [kg/m^3]	Diameter [mm]	Length [m]
Striker	Steel	7655	78.50	2
Output Bar	Nylon	1145	81.70	8.923

Table 9: Characteristics of the tubes tested with the blockbar

Tube	Length [mm]	Diameter or area	Weight [g]	Medcork reference	Average strain rate [s^{-1}]
T50VD21	50.00	110.74 mm^2	15.57	-	100
T50AD23	50.00	25 mm	21.44	B20	100
T50NRD11	50.00	25 mm	18.90	C5	100
T50RD21	50.00	25 mm	18.72	H40+H51	100

Table 10: Properties of the dynamic cork samples, for each Medcork reference.

Reference	Type of cork	Average diameter [mm]	Ovality [mm]	Density [kg/m^3]	Humidity [% HR]
A3	MA	22.86	0	294	6
A5	MA	22.84	0.02	297	6
A18	MA	22.89	0.01	291	6
B3	A	22.84	0.04	295	6.4
B18	A	22.82	0.04	294	6.4
B20	A	22.83	0.02	281	6.3
C5	NR	22.82	0.01	165	9.7
D2	A	22.85	0.01	299	6.3
D3	A	22.8	0.02	293	6.5
E3	NR	22.78	0.03	165	9.7
E4	NR	22.78	0.09	167	10.2
E9	NR	22.84	0.1	155	10.2
E11	NR	22.78	0.04	188	10.2
E12	NR	22.72	0.07	173	7
H19	R	22.74	0.02	152	9.7
H23	R	22.73	0.06	171	7
H40	R	22.8	0.04	147	9.9
H51	R	22.79	0.02	165	6.9
I2	MA	22.86	0.02	292	6
I3	MA	22.84	0.02	298	6

Table 11: Cork properties used in the numerical model.

	ρ [kg/m^3]	E (compacted) [GPa]	ν (compacted)	σ_y (compacted) [MPa]	Scale factor
Micro-agglomerate	293	9	0.3	1	3
Agglomerate	293	9	0.3	1	2
Radial	180	9	0.3	1	2
Non-radial	180	9	0.3	1	2.5

forces and velocities for each face of the sample. The speed of the striker was fixed to 5.5 m/s. Tables 8 to 10 refer to the characteristics of the tests realized with the blockbar.

3 NUMERICAL SIMULATIONS

Initially, the dynamic uniaxial compression tests realized experimentally with cork and tubular structures were simulated. In order to extend the numerical study to structures that could be used for industrial applications such as car industry, the authors also simulated the effects of agglomerate cork-filling in square aluminium tubes with 500 mm length. The geometrical models used in the modelling were created with the pre-processor ETA Femb and then exported to carry out numerical solutions with LS DYNA™, version 970. The visualization tool processor used was ETA PostGL and ETA Graph.

3.1 Properties of the Materials

For the different types of cork, the material used was `26.1.*MAT_HONEYCOMB`. This material is adequate to honeycomb and foam materials with real anisotropic behaviour. The behaviour before compaction is orthotropic where the components of the stress tensor are uncoupled, *i.e.*, a component of strain will generate resistance in the local a-direction with no coupling to the local b and c directions. The elastic moduli vary from their initial values to the fully compacted values, linearly with the relative volume (defined as the ratio of the current volume to the initial volume). For fully compacted material, it is assumed that the material behaviour is elastic-perfectly plastic. The parameters introduced were the density ρ, the Young modulus E, the Poisson coefficient ν and the compacted material yield stress σ_y, as well as the stress-strain curve of the cellular material for similar loadings. The model also allows to import a scale factor curve (function of the strain rate) in order to take into account the effect of the increase or decrease of strain rate. Thus, the Table 11 summarizes the average values of the parameters introduced for each type of cork. Some of them were the result of experimental conclusions whereas others were found in the literature [10].

The stress-strain curve imported was obtained from the static experimental tests of each type of cork, and the scale factor introduced is an average value observed during the dynamic experimental tests. The Young modulus for the material (before compaction) was set to 15 MPa, as a result of the experimental values observed.

The circular tubes tested experimentally with and without cork, and the square aluminium tubes were modelled with the material `24.1.*MAT_PIECEWISE_LINEAR_PLASTICITY`. This material models an elastic-plastic material with an arbitrary stress-strain curve and an arbitrary strain rate dependency can be defined.

Table 12: Properties of the aluminium alloys used in the numerical model.

	ρ [kg/m^3]	σ_y [MPa]	E [MPa]	ν
Al6060-T5	2710	160	61500	0.33
Al7075-O	2810	103	71700	0.33

For the circular tubes (EN AW 6060/6063-T5), the data from the tensile curve previously defined were used. For the square tubes, the properties of the aluminium alloy Al7075-O as well as the stress-strain curve, represented in Figure 8, were introduced (Table 12).

Strain rate was accounted for, using the Cowper-Symonds model which scales the yield stress of the material with the factor $\left[1+\left(\frac{\dot{\varepsilon}}{C}\right)^{1/P}\right]$, where C and P are constants depending on the material. For aluminium alloys, the values adopted were $P = 4$ and $C = 6500$ s^{-1}.

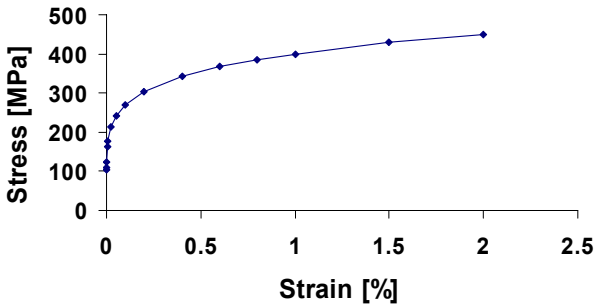

Figure 8: Stress-strain curve for the aluminium alloy Al7075-O.

3.2 Numerical Modelling

For the compressive simulations of cork, a typical cylinder with a diameter of 23 mm and a length of 25 mm was drawn. Initially, only one quarter of the section of the cylinder was meshed with 3-line mesh, dividing each line into 10 elements. To guarantee a symmetric mesh, 2 mirrors of the elements were made as well as a drag mesh along the length to form 25 layers of elements. A total of 2200 elements were defined.

The meshing consisted of 8-nodes hexahedral solid elements with 8 nodes and 3 degrees of freedom per node, for 8 points of integration (complete integration, with no problems of hourglass). The circular aluminium tubes under compressive loading were drawn by their middle surface. Half of the tube was meshed with the 4-line function (20 tangential and 25 longitudinal divisions) and the elements were then mirrored to duplicate the number of elements to the second half of the tube. A total of 1000 elements were defined (Figure 9). The elements used were Hugues-Liu shell elements, with 7 integration points along the thickness and 1.5 mm thickness at each node.

For the circular tubes filled with cork (of the four types), the cylindrical cork-filler had an outer diameter that was slightly larger than the inner diameter of the empty tube, in order to simulate correctly the experimental test.

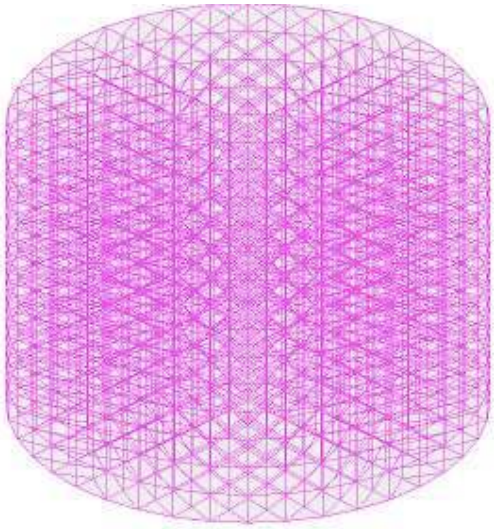

Figure 9: Cork mesh.

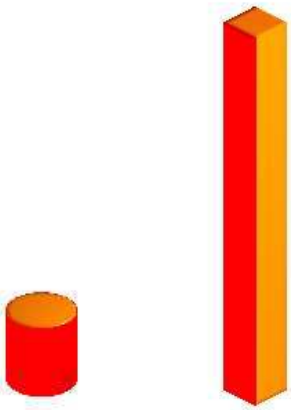

(a) (b)

Figure 10: Geometrical models of the tubes: (a) cork-filled circular tube (b) a quarter cork-filled square tube.

The square tubes modelled had a length of 500 mm, and a section with a side of 106 mm and a thickness of 3 mm. Only one quarter of the tube was considered, so it was necessary to define two symmetry planes. An automatic topology mesh of the section with 5 mm-size elements and a drag mesh along the length were performed. The same hexahedral 8-node solid elements were used. No gap was introduced between the cork and the tube. For these square aluminium tubes, only agglomerate and micro-agglomerate cork fillers were simulated given that the types of cork previously tested (R and NR) cannot be obtained in such shapes and dimensions. The boundary conditions adopted for the materials subjected to compressive loading correspond to the introduction of two rigid walls (modelled as rigid bodies) placed next to the base and upper section of the samples. One of the rigid walls is immobile whereas the other compresses the material while associated to a mass and a velocity.
For the cork and the circular tubes models, the velocities introduced correspond to the impact velocities experimentally tested, and the mass is equal to the weigh of the input bar (nylon or aluminium depending on the material) or to the weigh of the steel striker (for the simulations of the blockbar).
The Table 13 summarizes the velocities and masses associated to the moving rigid wall which impacts the structure.

Table 13: Characteristics of the moving rigid wall.

	Rigid wall velocity [m/s]	Wall mass [kg]
Cork	3.00	4.50
Circular tubes	11.00	10.25
(L=25mm)	15.00	10.25
Circular tubes	5.53	100.00
(L=50mm)		
1/4 square tubes	10.00	125.00
	15.00	125.00

For each tubular structure (with or without filler), the `Automatic_Surface_to_Surface` contact of the LS-DYNA library was used to prevent self-penetration of the tubes and to avoid the mutual penetration of the two coupled materials. For the tubes, displacements and rotations of the nodes in contact with the compression rigid walls were not allowed, except the displacement of the upper nodes along the vertical axis.

4 RESULTS AND DISCUSSION

4.1 Cork

The cork stress-strain curves resulting from the static tests are presented in Figure 11. The slight jump visible in all the static curves for a stress of approximately 4 MPa is due to a small deficiency in the testing machine. Independently of the cork type and of the Medcork characteristics of each specimen (humidity, ovality, density), the static curves obtained for each series of three samples were identical.
Moreover, the static results for 15 and 20 mm samples are also identical, as shown in Figure 12, where stands a comparison between the average stress values of each sample for each type of cork. Those similar static results allow to justify the use of the static stress-strain curve as a reference input stress-strain curve for numerical calculations.

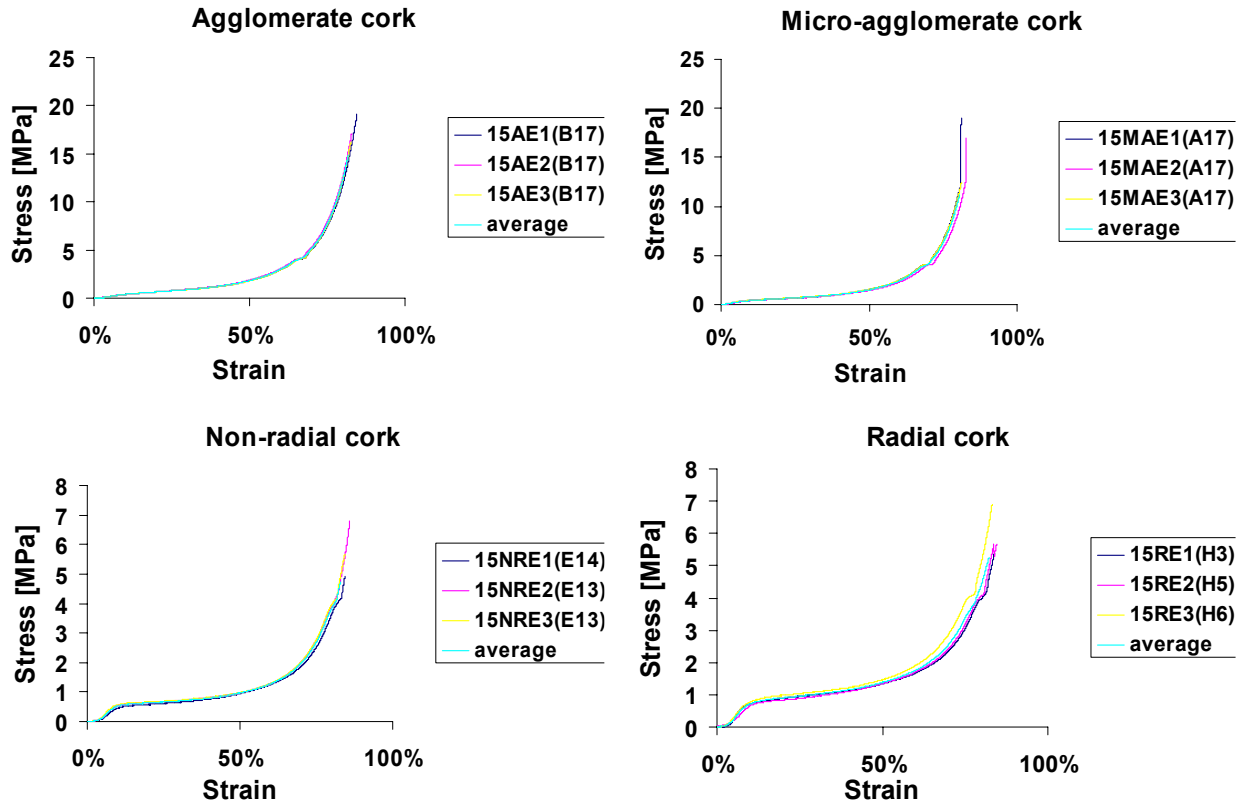

Figure 11: Static stress-strain curves for the 15 mm cork samples.

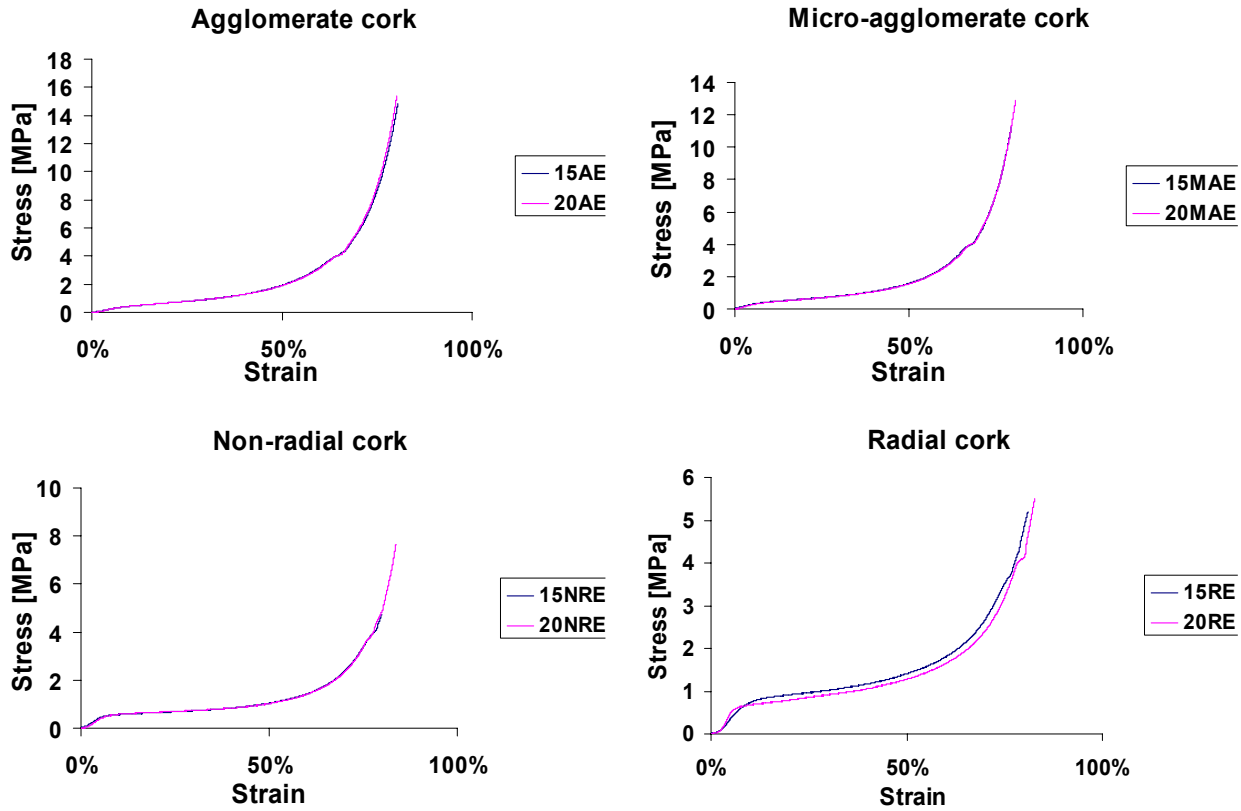

Figure 12: Comparison of the static stress-strain curves for 15 mm and 20 mm cork samples.

In Figure 13, the stress-strain curves obtained for each type of 15 mm cork sample are shown.

Each curve presents an elastic part, mainly as a result of the cell walls and edges bending. After that, elastic collapse gives an almost horizontal plateau for a stress of 1 MPa: the cells collapse is mainly due to cells walls crushing. Actually, a real horizontal plateau does not exist (the stress grows slightly during the collapse propagation in cork) due to the structure heterogeneity. Finally, the complete collapse of the cells causes the curve to rise steeply at about 70% strain, when the cells walls start to touch each other.

It appears that the static Young modulus of radial and non-radial cork is higher than the one of agglomerate and micro-agglomerate cork. The static Young modulus values are estimated to 29 MPa for radial and 19 MPa for non-radial cork. Fortes *et al.* [10] refer to an increase of the modulus with density. Nevertheless, in this work, the discrepancy between density values of the samples tested seem to be insufficient to show this tendency. For low strains, natural cork (radial in particular) supports higher values of stress, but after 30% strain, the agglomerate are more resistant (in particular micro-agglomerate cork).

To analyse the deformation uniformity in the natural cork samples statically tested, a regular grid was drawn in one of the samples. During the test, a progressive distortion of the grid was observed, demonstrating that deformation is not uniform, mainly near to the cracks and pores which constitute the lenticular channels and whose distribution in cork is irregular (Figure 14). However, deformation is uniform for agglomerate cork samples.

The Figure 15 shows the dynamic stress-strain curve for each type of cork samples.

Agglomerate cork as well as micro-agglomerate cork present similar values, regardless of the sample tested characteristics and of the strain rate. These observations allow to conclude that the variation of strain rates, for the range considered (200 to 600 s^{-1}), does not have influence on the mechanical behaviour of the agglomerates. However, the dynamic plateau stress is higher than the static one, so agglomerates are not at all materials whose behaviour is independent from the strain rate applied.

Regarding non-radial and radial cork, the differences between static and dynamic results are much more significant. For non-radial cork, the value of the plateau stress changes with the sample, between 1 MPa and 1.5 MPa. There does not seem to exist a direct relation between the plateau stress and the strain rate, since some samples such as NRD12 and NRD14 present the highest value of plateau stress in spite of being tested at the lowest strain rate values. The relevant points seem to be the microstructure and the properties of the tested sample. Indeed, the samples which present similar plateau stress (and similar stress-strain curves) are those which were cut off from the same initial sample (thus having the same Medcork reference). Hence, the authors can conclude that there may be a strong influence of the microstructure on the mechanical behaviour since samples made of neighbour cells present the same mechanical curve. As a consequence, the exact prevision of the dynamic behaviour of any sample of natural cork under compressive loading seems to be a major difficulty, mainly because cork microstructure varies with the region of the cork-oaks plantation, with the cork-oak, and even inside the same corktree. In fact, the thickness, the inclination, and the number of corrugations in the cells can be relevant for its mechanical behaviour. Moreover, the high variability of density values can be affected by humidity and also depend on the cork type. Density gradients can be present on the same piece of cork: autumn and spring cells also have different shapes and thicknesses.

For radial cork, the plateau stress varies from 0.5 to 2 MPa approximately. This cork type also presents the same results for samples obtained from the same original specimen, which may suggest that, once more, the mechanical behaviour of radial cork depends on the microstructure. However, there does not seem to be a linear influence of the samples density or humidity on their mechanical behaviour (Figure 16).

Comparatively with the static behaviour, non-radial cork presents higher values of dynamic plateau stresses. This behaviour can be a consequence of inertial effects on the cell walls when those are impacted at high strain rates. However, radial cork seems to have a slightly different behaviour since the increment of the plateau stress is not observed for all the tested samples. Some of them, such as RD16, present a plateau stress equal to the static one. This particular feature may be due to the cells shape in the radial direction (concertina shape), which may explain the crushing mode of the walls in the radial direction and thus, the inferior value of the compressive stress.

The Figure 17 shows the difference between the stress-strain curves obtained for each type of cork, when impacted twice at the same strain rate. For all types of cork, except radial cork, lower values of plateau stresses and Young moduli are observed for the second impact. This result suggests a degradation of the cells occurred during the first impact.

For radial cork, the shape of the stress-strain curve does not change. Once more, this fact may be a consequence of the cells shape on the radial direction, which may explain that there is no explicit degradation of the cells.

The numerical simulations results for the dynamic tests of the cork are shown in Figure 18. Numerical and experimental results show quite good agreement up to the strain value considered.

4.2 Circular Tubes

The static analysis shows that independently of the tube length and the cork type used as filler, there are no significant differences between the stress-strain curves for the different tested samples (Figure 19).

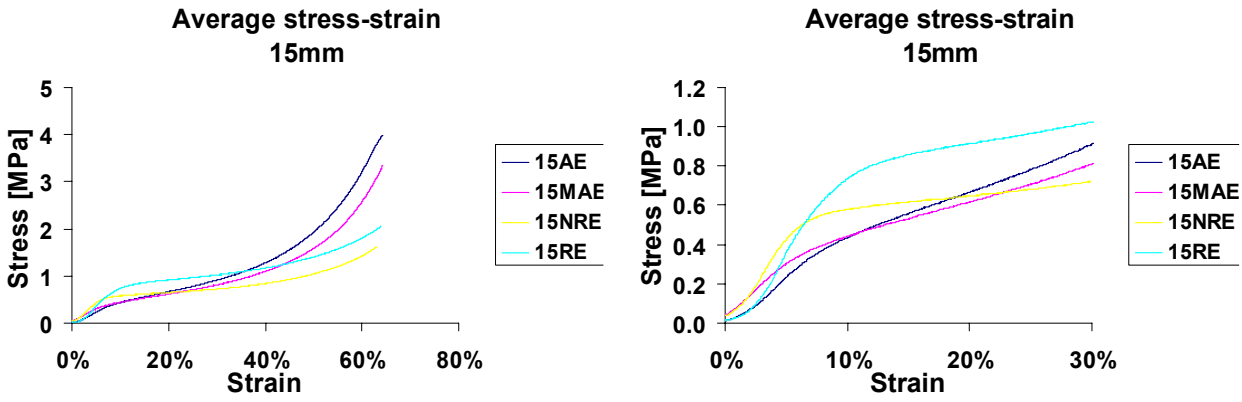

Figure 13: Average stress-strain curves for each type of cork.

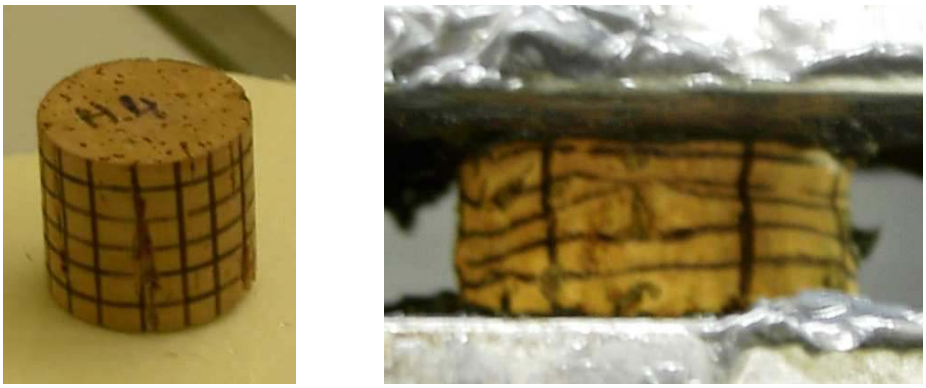

Figure 14: Evidence of a non-uniform deformation of natural cork.

Some differences are observed but only after 50% strain, and tubes filled with agglomerate and micro-agglomerate cork show higher values of forces than the others.

For both types of dynamic tests, those realized with aluminium SHPB, and those tested with the block-bar, the difference between the forces supported by the different structures is not significant for the range of displacements considered (Figures 20 and 21).

Moreover, no significant differences were observed between static and dynamic results.

The observation of the impacted samples allowed us to conclude that there was no modification of the deformation modes of the tubes after filling them with cork, possibly because of the value of the diameter/thickness ratio. The samples which show more deteriorated cork are the ones filled with natural cork (characterized by the presence of more defects).

A significant, but not complete, recuperation of the cork filler size was observed after impact as a result of the viscoelastic component of cork deformation (Figure 22).

The numerical simulations carried out with LS-DYNA™ software show a quite good agreement with the available experimental results, concerning stress-strain curves (Figure 23).

The numerical results calculated for 11 and 15 m/s suggest a slight influence of the cork filler on the force and kinetic energy of the several structures (Figure 24), but only for high values of strain (approximately 50%), as observed experimentally.

The deformation modes observed experimentally and numerically are also very similar (Figure 22). The simulations of the tests performed with the block-bar showed that, in average, the forces calculated for each sample follow the tendency of the experimental results and allow to confirm that the presence of cork as a filler inside circular aluminium tubes with the shape and characteristics of the ones tested experimentally does not bring relevant advantages in terms of energy absorption (Figure 25).

4.3 Square Tubes

From the observation of the force-displacement curves of the Figure 26 for 10 m/s and 15 m/s impacts, the authors concluded that the forces calculated for cork-filled structures are higher than the ones of the empty tubes. Moreover, agglomerate and micro-agglomerate cork show similar results. At 10 m/s, the average force increases from 35 kN to 45 kN, and at 15 m/s, it increases from 30 kN to 50 kN (meaning that there is an increase of 70% at 15 m/s).

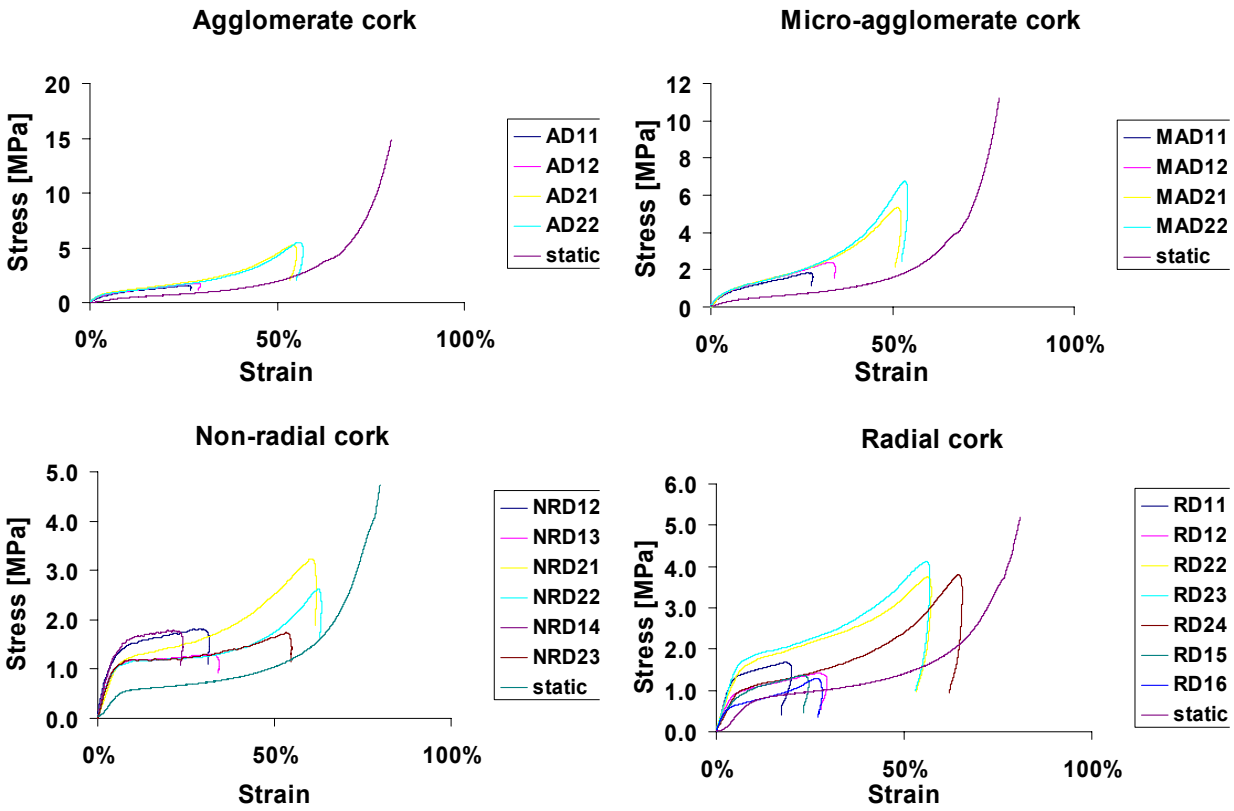

Figure 15: Static and dynamic stress-strain curves for each type of cork.

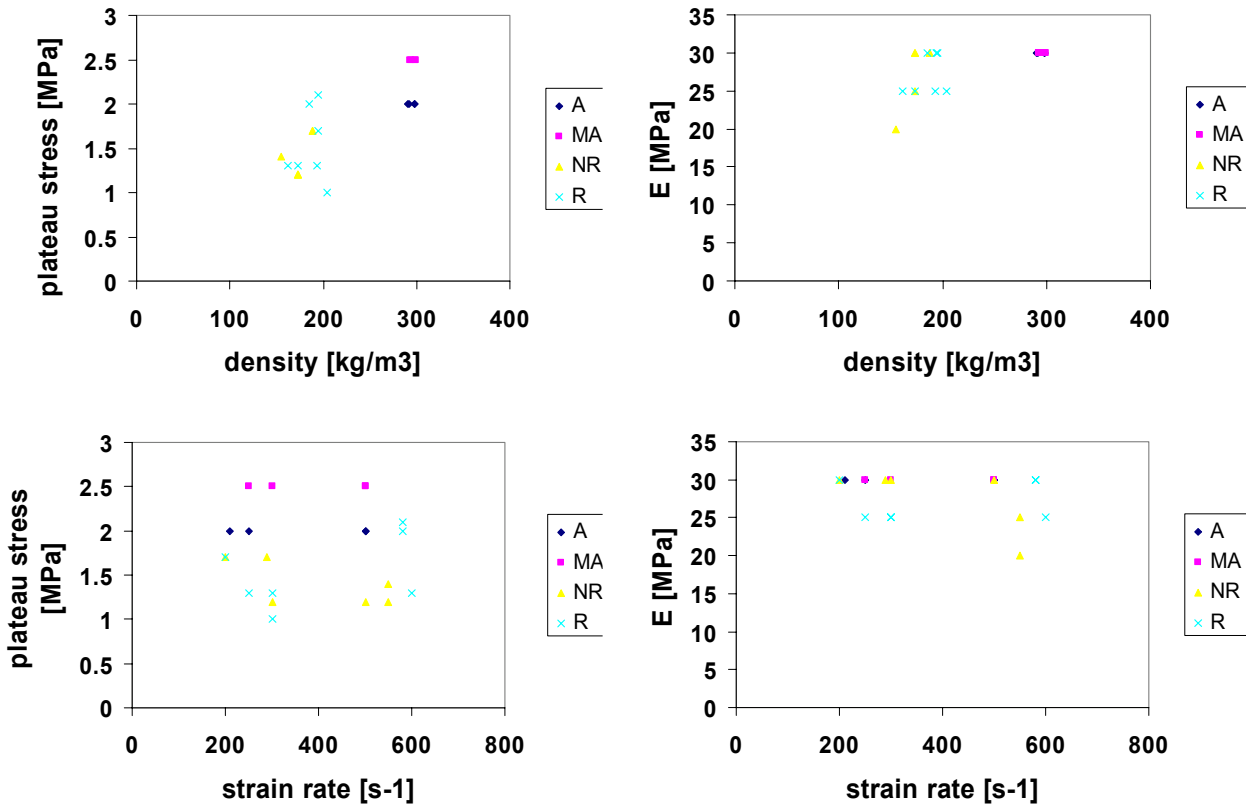

Figure 16: Influence of the strain rate and the density on plateau stress and Young modulus for each type of cork.

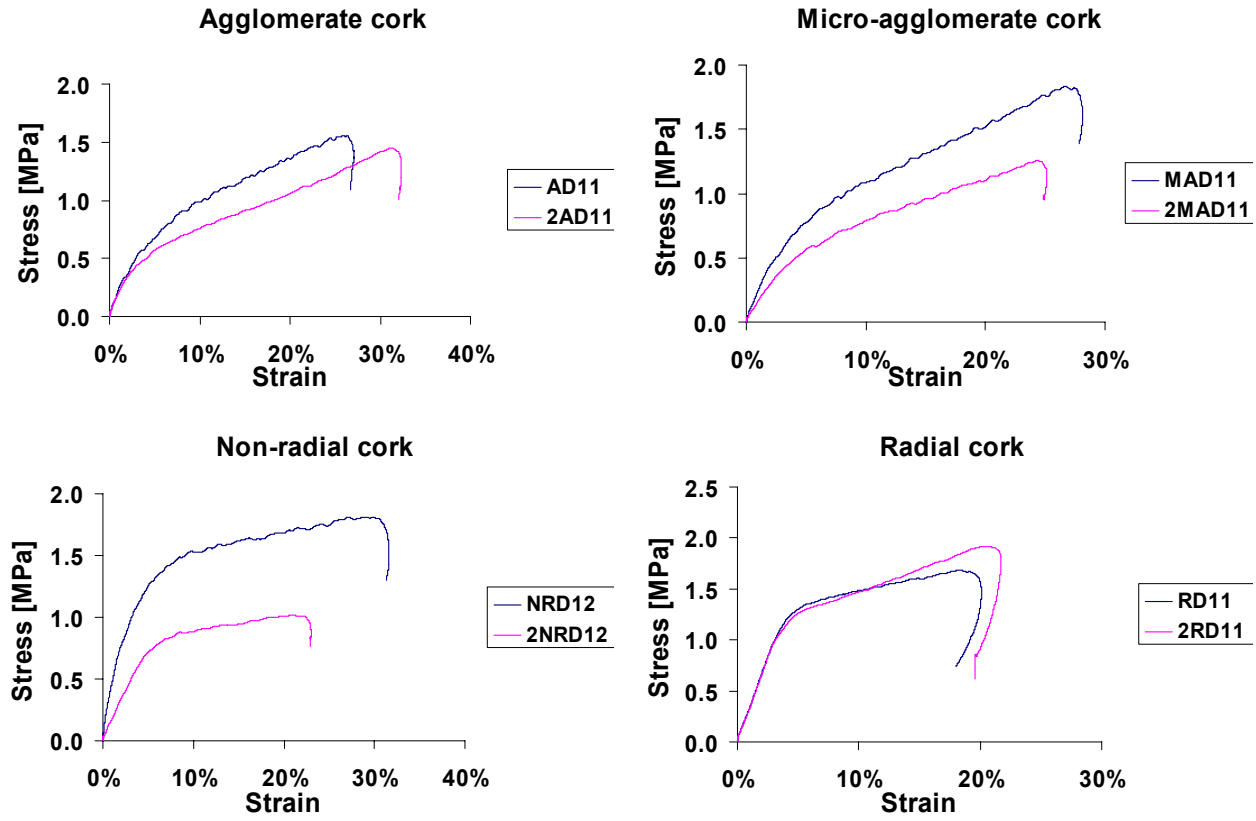

Figure 17: Stress-strain curves after a second impact on the same cork sample. The pink curve represents the cork behaviour after the second shot.

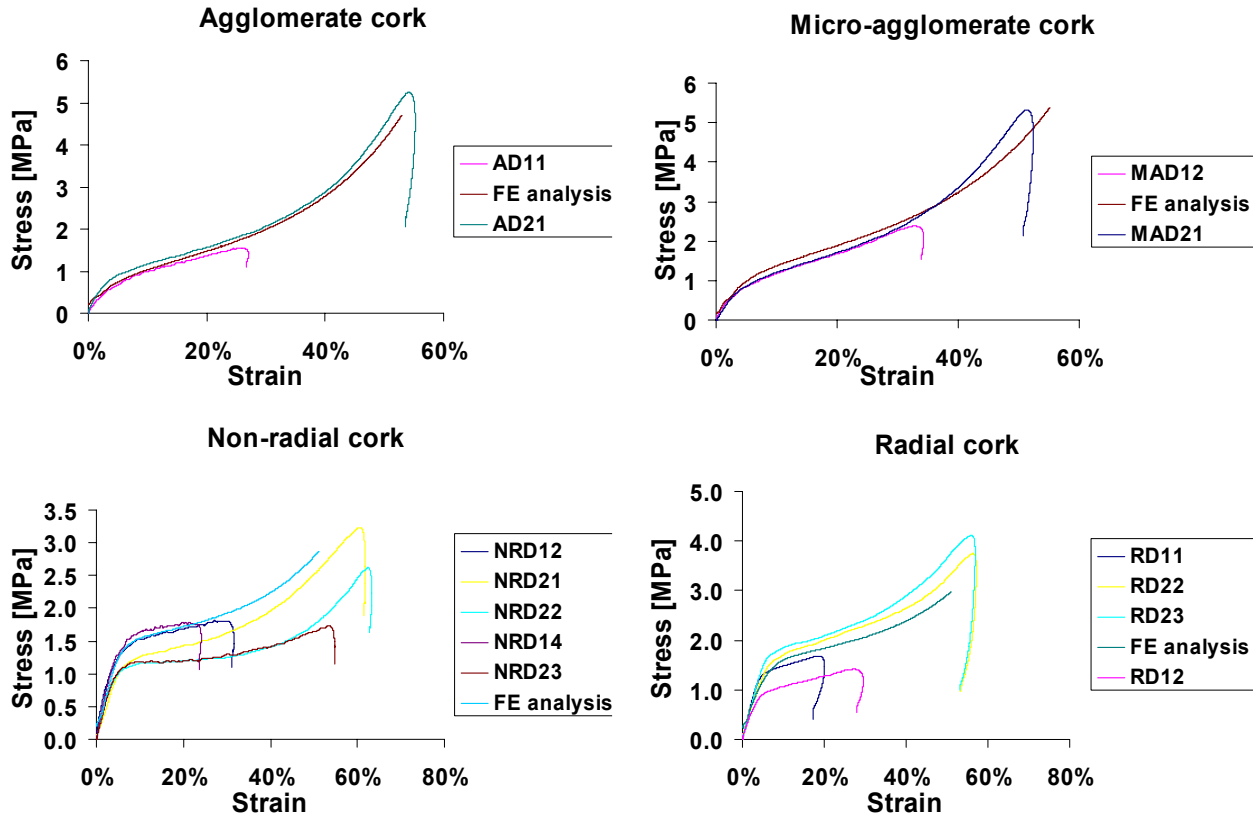

Figure 18: Comparison between experimental and numerical stress-strain curves obtained for cork.

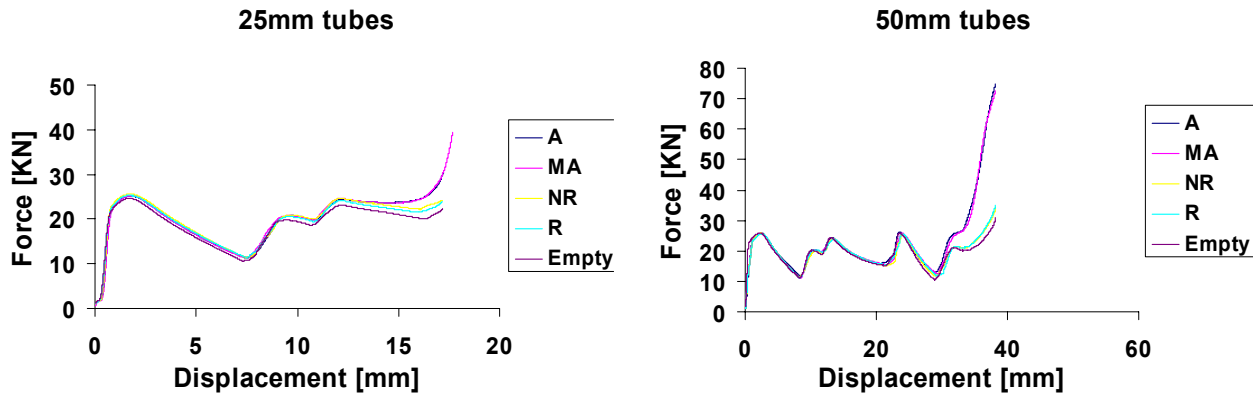

Figure 19: Static force-displacement curves for the circular aluminium tested tubes.

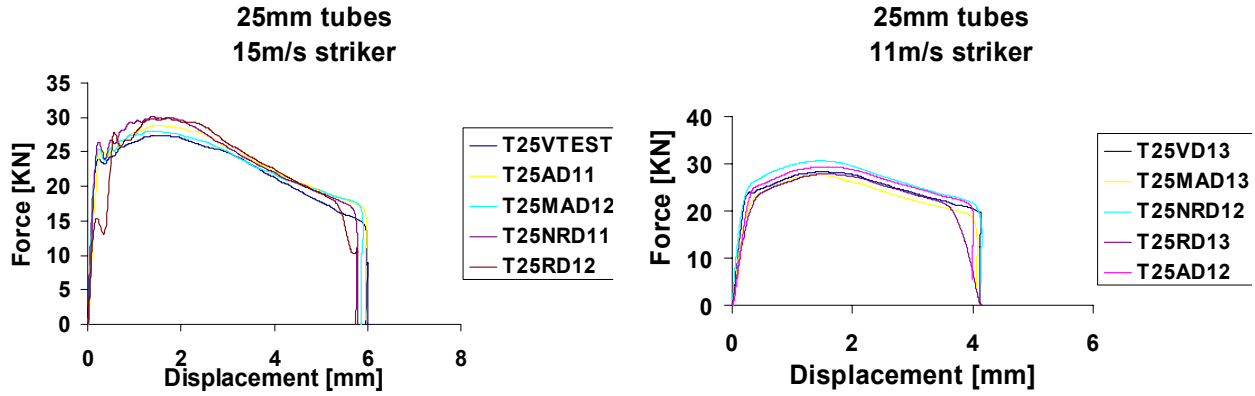

Figure 20: Dynamic force-displacement curves for the circular tubes tested with aluminium SHPB at 11 m/s and 15 m/s impact speeds.

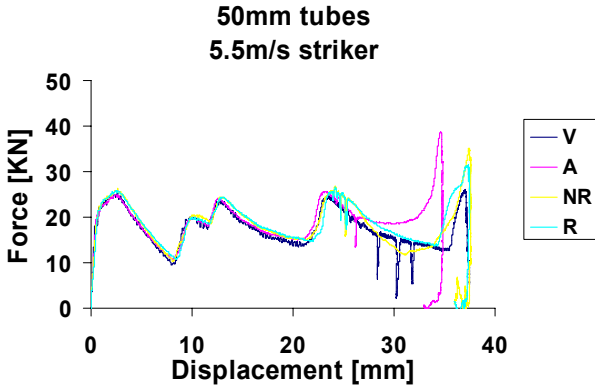

Figure 21: Force-displacement curves of the tubes tested with the blockbar.

(a) (b)

Figure 22: Samples geometry after 15 m/s impact – (a) experimental – (b) numerical.

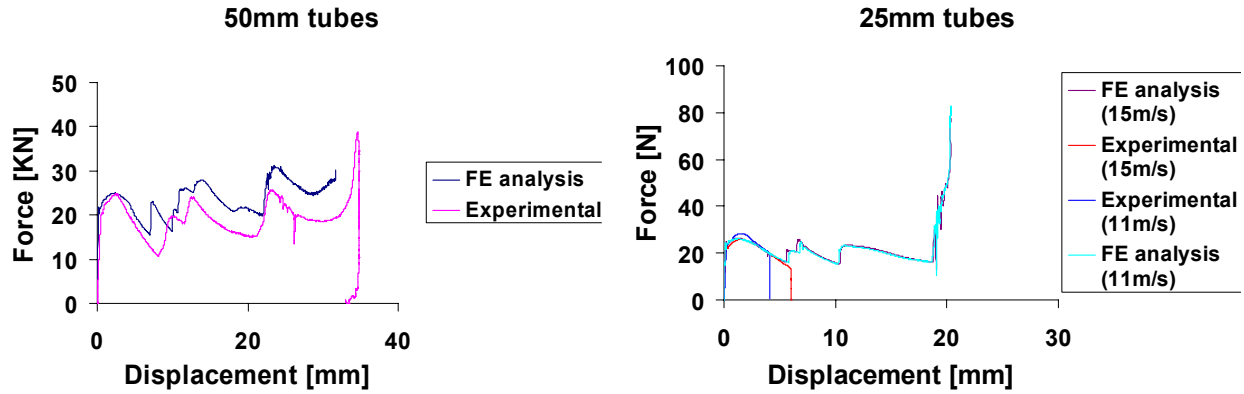

Figure 23: Comparison between the numerical and experimental force-displacement curves for the 25 mm and 50 mm circular tubes.

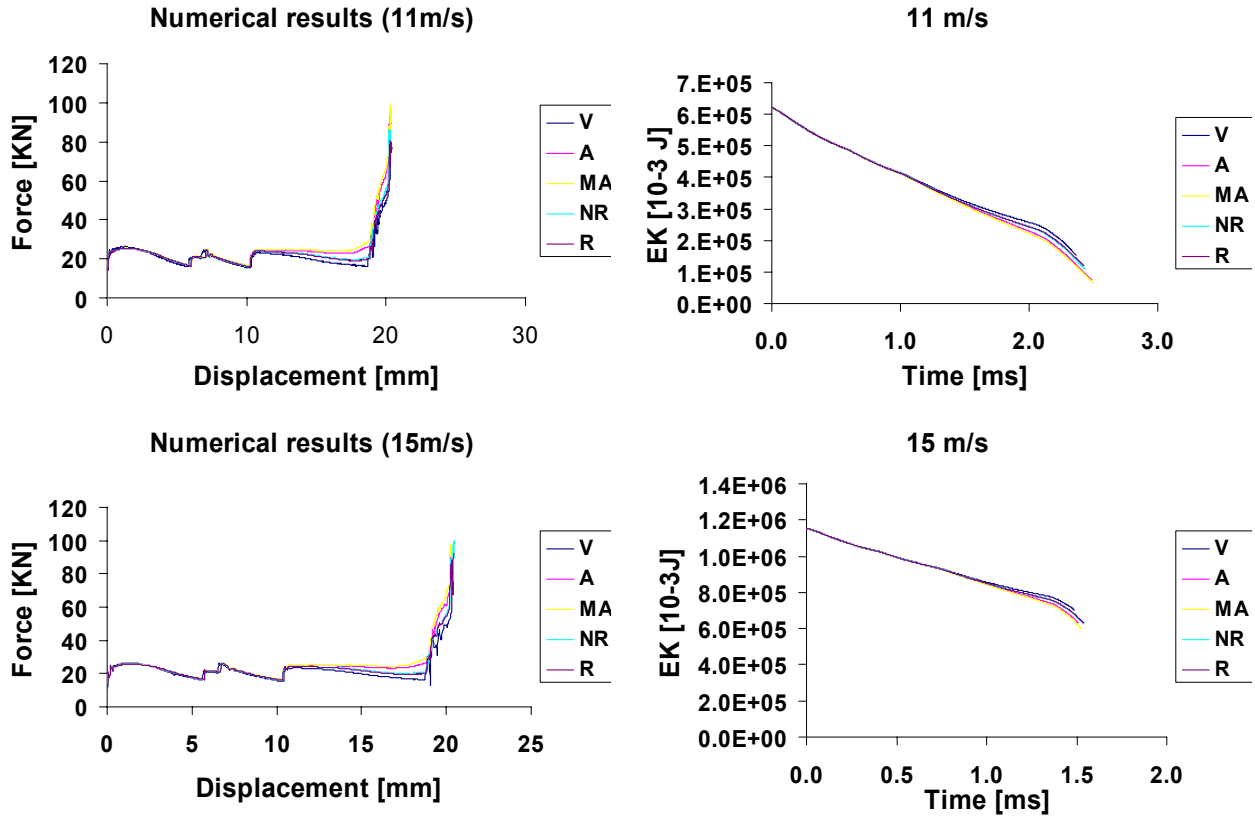

Figure 24: Numerical force-displacement curves and kinetic energy vs time, for the different types of tubes after 11 and 15 m/s impact.

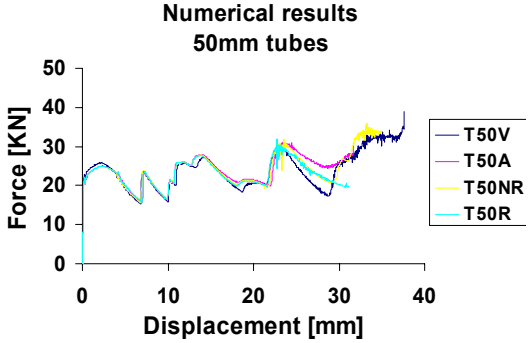

Figure 25: Numerical force-displacement curves for 50 mm tubes tested with the blockbar.

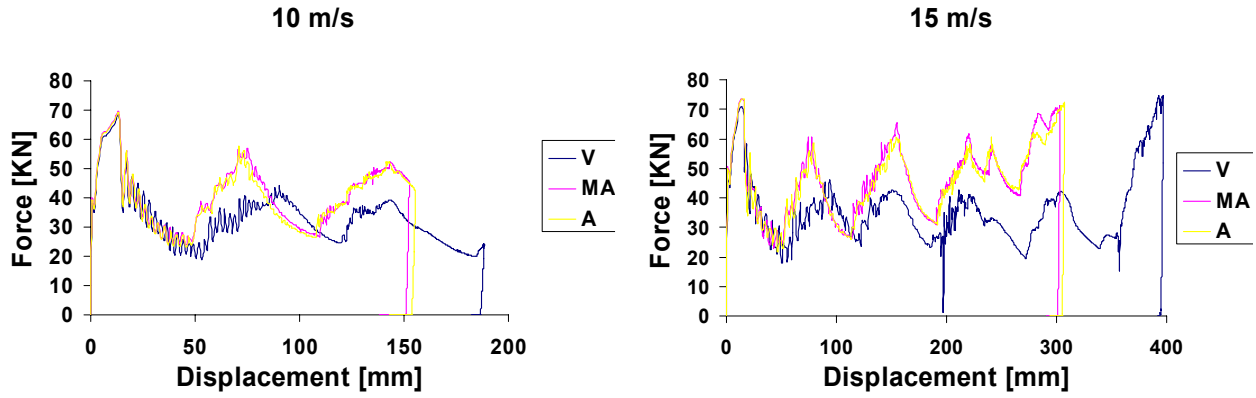

Figure 26: Numerical force-displacement curves for the square tubes after 10 and 15 m/s impact.

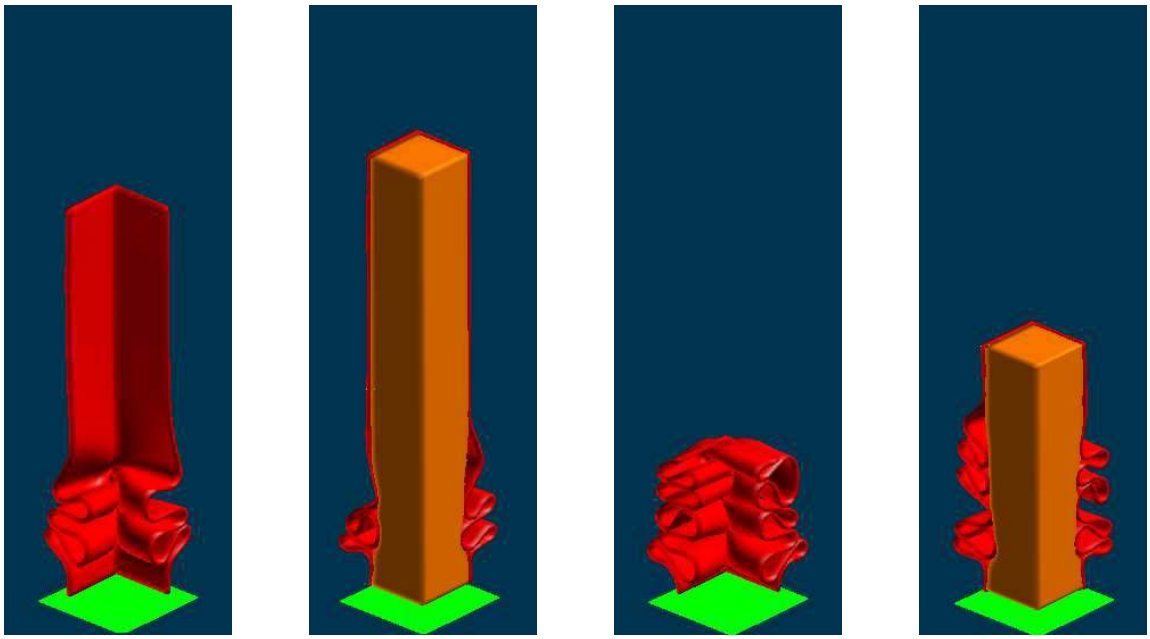

(a) (b) (c) (d)

Figure 27: Final geometry of the tubes without (a) and with cork (b) a 10 m/s impact, and without (c) and with cork (d) a 15 m/s impact.

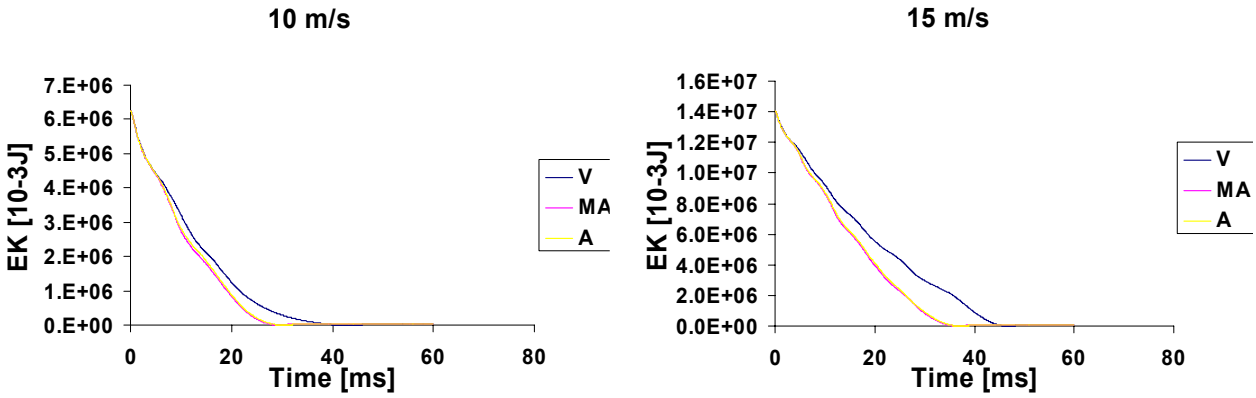

Figure 28: Kinetic energy variations of the tube with time after a 10 m/s and a 15 m/s impact.

The return of the force to zero corresponds to the moment when the impacted structure separates from the immobile rigid wall after rebound. Thus, for both impact speeds, a clear diminution of the value of the final strain is observed for the structures containing cork: at 15 m/s, it decreases from 390 mm to 300 mm, and at 10 m/s, it decreases from 185 mm to 150 mm, allowing to gain approximately 19% deformation at 10 m/s and 23% at 15 m/s. This fact also corresponds to a lowest number of folds in the filled tubes, as shown in the Figure 27.

The Figure 28 shows the variations of the kinetic energy with time. The obtained values show a clear increase of the absorbed energy for the structures containing cork.

The Figure 29 compares the global velocity of the structure in the impact direction, as a function of the elapsed time after impact.

At 10 m/s, the cork-filled structure stops 30 ms after impact, while at the same moment the identical empty structure still moves at 2 m/s, and will stop only 43 ms after the impact. At 15 m/s, the empty tubes reach a null global velocity after 47 ms, while the filled structure lasts 37 ms to stop. Moreover, when the cork filled structure stops, the unfilled tube is still moving at 6 m/s. The Figure 30 summarizes the benefits of the introduction of cork.

It is important to enhance the fact that the introduction of cork almost corresponds to an insignificant increase of the structure mass (due to its low density), which allows to hope that cork may be used in new applications involving specific energy-absorbing systems.

5 CONCLUSION

The dynamic behaviour of cork has been studied experimentally and numerically, alone, and used as filler inside aluminium tubes. The numerical simulations of impact tests were realized with LS-DYNA™ finite element software and showed quite good agreement with the experimental results, suggesting it may be doable to predict in average the mechanical behaviour of cork-filled structures under dynamic loading.

There are many application fields that have not been explored yet for the use of cork, possibly due to the fact that it is a complex cellular material, characterized by very variable mechanical properties which clearly depend on its microstructure.

Depending on the structure considered, using cork as a filler can be either indifferent, either positive. The authors observed that for the square aluminium tubes studied, agglomerate and micro-agglomerate cork brings obvious advantages in terms of deceleration and energy absorption. Moreover, cork is cheap and light, in comparison with some metallic foams, which could give an impulse to its use in new lightweight absorbing structures.

Actually, the analysis of the benefits of the introduction of cork is far from trivial since it involves the type of application (defining geometrical, material and project limitations), the criterion used to evaluate performance (energy absorption per unit of mass, energy absorption per unit of volume, maximum force compared to energy absorption, deceleration, final deformation of the structure, etc) and, of course, the characteristic parameters of the structure (filler material and density, width, thickness and length of the tube, shape of the section, tube material, etc.)

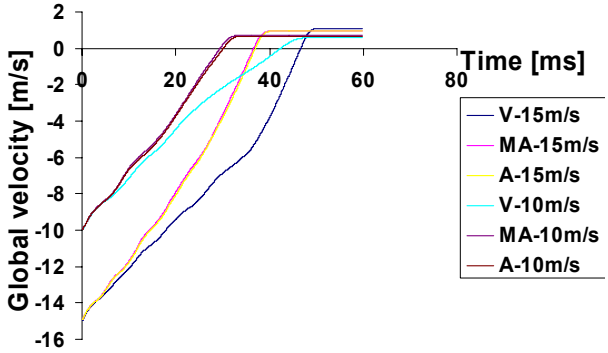

Figure 29: Evolution of the tubular structures global velocity with time for 10 and 15 m/s impact.

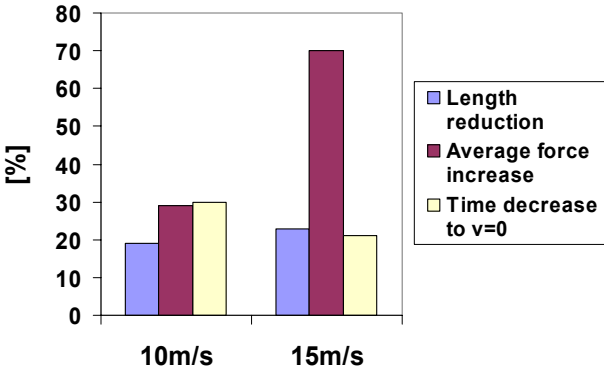

Figure 30: Benefits of the introduction of cork in the square tubes for 10 and 15 m/s impacts.

ACKNOWLEDGEMENTS

The authors are grateful to the Portuguese Foundation for Science and Technology (FCT) who financially supported this work, through the Program POCTI /35907/EME/2000 (Portuguese Government and FEDER) and SFRH / BD / 18964 / 2004, and to ROCAP for providing the cork samples.

REFERENCES

[1] Gibson, L.J.; Ashby, M.F.; *Cellular Solids: Structure and Properties*, Second Edition, Cambridge University Press, Cambridge, U.K, 1997.

[2] Deshpande, V.S.; Fleck, N.A.; High Strain Rate Compressive Behaviour of Aluminium Alloy Foams, *International Journal of Impact Engineering* **24**: 277-298, 2000.

[3] Paul, A.; Ramamurty, U.; Strain rate sensitivity of a closed-cell aluminum foam, *Materials Science and Engineering* **A281**: 1-7, 2000.

[4] Santosa, S.P.; Wierzbicki, T.; Hanssen, A.G.; Langseth, M.; Experimental and numerical studies of foam-filled sections, *International Journal of Impact Engineering* **24**: 509-534, 2000.

[5] Hall, I.W.; Ebil, O.; Guden, M.; Yu, C.-J.; Quasi-static and dynamic crushing of empty and foam-filled tubes, *Journal of Materials Science* **36**: 5853-5860, 2001.

[6] Hanssen, A.G.; Langseth, M.; Hopperstad, O.S.; Static and dynamic crushing of circular aluminium extrusions with aluminium foam filler, *International Journal of Impact Engineering* **24**: 475-507, 2000.

[7] Kavi, H.; Toksoy, A.K.; Guden, M.; Predicting energy absorption in a foam-filled thin-walled aluminum tube based on experimentally determined strengthening coefficient, *Materials and Design*, 2004.

[8] Toksoy, A.K.; Guden, M.; The strengthening effect of polystyrene foam filling in aluminium thin-walled cylindrical tubes, *Thin-Walled Structures* **43**: 333-350, 2005.

[9] Aktay, L.; Toksoy, A.K.; Guden, M.; Quasi-static axial crushing of extruded polystyrene foam-filled thin-walled aluminum tubes: Experimental and numerical analysis, *Materials and Design*, 2005.

[10] Fortes, M.A.; Rosa, M.E.; Pereira, H.; *A Cortiça*, IST Press, 2004.

[11] Anjos, O.; Pina, P.; Rosa, M.E.; *Comportamento mecânico da cortiça em compressão e sua relação com a porosidade*, Actas da European Conference on Cork Oak and Cork, pp 317-325; Lisboa: Centro de Estudos Florestais - Instituto Superior de Agronomia, 1997.

[12] Fortes, M.A.; Nogueira, M.T.; The Poisson effect in cork, *Material Science and Engineering*, **A122**: 227-232; 1989.

[13] Gibson, L.J.; Easterling, K.E.; Ashby, M.F.; *The structure and mechanics of cork*, Proc. of the Royal Society of London, **A377**: 99-117; 1981.

[14] Gary, G.; *Some Aspects of Dynamic Testing with Wave-Guides*, New Experimental Methods in Material Dynamics and Impact, Trends in Mechanics of Materials, Volume 3, Nowacki, W.K. and Klepaczko, J.R. (Eds.), pp 179-222; INB ZTUREK, P.O. Box 374, 00-950 Warsaw 1, Poland, 2001.

[15] Zhao, H.; Gary, G.; Klepaczko, J.R.; On the use of a viscoelastic split Hopkinson pressure bar, *International Journal of Impact Engineering*, **19**: 310-330; 1997.